Available online at www.sciencedirect.com
ScienceDirect
Chemical Geology 249 (2008) 250–261
CHEMICAL GEOLOGY INCLUDING ISOTOPE GEOSCIENCE
www.elsevier.com/locate/chemgeo

Solubility of corundum in the system Al_2O_3–SiO_2–H_2O–NaCl at 800 °C and 10 kbar

Robert C. Newton, Craig E. Manning*

Department of Earth and Space Sciences, University of California Los Angeles, Los Angeles, CA 90095-1567, USA

Received 12 March 2007; received in revised form 7 January 2008; accepted 8 January 2008

Editor: R.L. Rudnick

Abstract

The solubility of corundum was measured at 800 °C and 10 kbar in NaCl–H_2O–SiO_2 fluids over NaCl mole fractions (X_{NaCl}) of 0 to 0.5 and SiO_2 concentrations of zero to quartz or albite + melt saturation, depending on X_{NaCl}. Experiments were performed in a piston-cylinder apparatus. Dissolved Al_2O_3 and SiO_2 were determined by weight losses of corundum and quartz crystals, or by bulk compositions of bracketing experiments. Although kyanite and sillimanite are slightly more stable than corundum + quartz at these pressures (*P*) and temperatures (*T*), neither appeared in any of the experiments. Results indicate that the enhancement of corundum solubility by NaCl at this *P* and *T* is further promoted by the addition of SiO_2. At quartz saturation, significant enhancement occurs in initially pure H_2O and addition of NaCl yields yet higher Al_2O_3 concentrations. At $0.03 \le X_{NaCl} \le 0.1$, quartz saturation is replaced by albite + silicate melt. The anhydrous melt composition is nearly on the join $NaAlSi_3O_8$–SiO_2. Al_2O_3 molality rises rapidly with NaCl concentration to 0.038 at $X_{NaCl} = 0.1$ and then increases more slowly to 0.052 at halite saturation. There is, in addition, a measurable reciprocal enhancement of Si solubility by virtue of dissolved Al at a fixed X_{NaCl}. Quench pH in NaCl-bearing fluids is strongly acidic and Na/Cl < 1 in quench solutes, suggesting low pH at high *P* and *T*. These observations, combined with previous work indicating Si–Al and Na–Al complexing, lead to the hypothesis that the reciprocal solubility enhancement of Al and Si is due to formation of Na-aluminosilicate complexes. Mass balance consideration suggests that the bulk Si/Al ratio of the group of complexes ranges from 1 to 2 in the NaCl-free system, to > 3 at high X_{NaCl}. Our data show that Al_2O_3 is a moderately soluble component in quartz + aluminosilicate-saturated rocks in the presence of intergranular salt solutions at deep-crustal metamorphic *P*–*T* conditions and commonly realized salinities. Al_2O_3 should not be regarded as a fixed reference component, because it may exhibit substantial mobility.

Keywords: Corundum solubility; Experimental petrology; Al mobility; Metamorphic fluids

1. Introduction

Among the major rock-forming components, alumina is commonly regarded to be among the least soluble in H_2O at high temperature (*T*) and pressure (*P*). For this reason, a fixed-Al_2O_3 reference frame has been used to model bulk chemical changes in high-grade metasomatism (Carmichael, 1969; Hansen et al., 1987). However, aluminosilicate parageneses have been described in which Al_2O_3 seems to have been quite mobile. Examples of Al_2O_3 transport include hydrothermally deposited veins in high-grade metamorphic rocks with quartz and an Al_2SiO_5 polymorph (Foster, 1977; Vernon, 1979; Mohr and Newton, 1983; Kerrick, 1988, 1990; Cesare, 1994; Ague, 1994; Nabelek, 1997; Whitney and Dilek, 2000; Widmer and Thompson, 2001; McLelland et al., 2002; Sepahi et al., 2004). However, the physico-chemical conditions under which Al_2O_3 can behave as a mobile component in rock systems at high *P* and *T* have not yet been adequately defined.

Mobility (i.e., the ability of components to segregate and concentrate) does not, in itself, require enhanced solubility in an intergranular fluid medium, but could just as well reflect high diffusive mobility through such a fluid. Several authors have

* Corresponding author.
E-mail address: manning@ess.ucla.edu (C.E. Manning).

0009-2541/$ - see front matter © 2008 Elsevier B.V. All rights reserved.
doi:10.1016/j.chemgeo.2008.01.002

argued that filling of veins in regional metamorphism could be accomplished by diffusion through a static intergranular medium without appealing to advective fluid flow or enhanced solubility (Fisher and Brantley, 1992; Cesare, 1994; Widmer and Thompson, 2001). Nevertheless, solubility enhancement by non-aqueous components of natural fluids, such as salts or alkaline complexes, must also have an effect on transport of Al_2O_3 (e.g., Anderson and Burnham, 1983).

The solubility of corundum, Al_2O_3, at 800 °C and 10 kbar in pure H_2O is only 0.0013 *m* (mol/kg H_2O; Tropper and Manning, 2007), compared to 1.3 *m* for quartz, SiO_2, at the same *P*–*T* conditions (Manning, 1994). However, addition of major rock-forming elements in various forms to aqueous fluids may dissolve Al_2O_3 in much greater amounts than does pure H_2O. Concentrated NaOH and KOH solutions greatly increase the solubility of corundum at high-grade metamorphic conditions (600–900 °C and 2–9 kbar: Anderson and Burnham, 1967); such highly basic solutions may not be commonly realized in nature, however. At high *P* and *T*, interaction with SiO_2 causes substantial increases in Al_2O_3 solubility (Manning, 2007). Highly soluble Al_2O_3 in the form of feldspar-like species exists at very high *P* and *T* near the liquid–vapor critical curve in the system $NaAlSi_3O_8$ (albite)–H_2O (800–900 °C, 12–17 kbar: Shen and Keppler, 1997). Addition of NaCl also increases Al_2O_3 solubility. Walther (2001) showed that NaCl solutions of low to moderate salinity (up to 0.5 *m*) greatly increase the solubility of corundum at 1 and 2 kbar and temperatures up to 600 °C, and Newton and Manning (2006) found that NaCl enhances the solubility of corundum by a factor of about 10 at 800 °C and 10 kbar. These findings offer the possibility of explaining enhanced Al_2O_3 mobility in typical crustal fluids at medium to high-grade metamorphic conditions by simply enhancing solubility to an extent that has previously gone unappreciated.

Of particular interest is the possibility that concentrated brines may be important in aluminosilicate–quartz vein formation. This is suggested by the study of McLelland et al. (2002) on the extensive sillimanite veining in the central Adirondack Highlands of New York, where quartz in veins contains concentrated saline fluid inclusions (up to 26 wt.% NaCl equivalent). It is possible that enhancement of Al_2O_3 solubility by dissolved salts could have been a factor in aluminum silicate vein emplacement. The role of brines in high-grade metamorphism remains uncertain and likely varies among settings — for example, brines may be generated or introduced during peak (Newton et al., 1998) or retrograde (Markl and Bucher, 1998) conditions. But regardless of origin and timing, the presence of brines makes it necessary to assess their ability to contribute to mass transfer processes attending metamorphism.

In light of the strong Al_2O_3 solubility enhancement afforded by addition of either NaCl or SiO_2 to H_2O at high *P* and *T*, it is likely that high concentrations of dissolved Al will exist in quaternary Al_2O_3–SiO_2–H_2O–NaCl solutions. However, no experiments on this system have previously been reported at deep-crustal conditions. The present study is a first attempt to define corundum and aluminum silicate solubilities as a function of SiO_2 activity and salinity at high *P* and *T* in the simple system Al_2O_3–SiO_2–NaCl–H_2O. The goal was to determine if Al_2O_3 solubility is enhanced by the presence of both SiO_2 and NaCl in solution. The results place constraints on the nature of interactions between crustal rocks and intergranular fluids, and shed light on the problem of Al_2O_3 transport in deep-crustal metamorphism.

2. Experimental methods

The experiments used synthetic corundum chips (1–7 mg) taken from a large boule (Newton and Manning, 2006). The chips were shaped into ellipsoids with a diamond file and smoothed with 600-mesh alundum paper and 15 μm diamond paper. Corundum grains plus natural Brazilian quartz (Newton and Manning, 2000) were encapsulated with reagent grade NaCl and nanopure H_2O in welded segments of Pt tubing of 3.5 mm diameter, ~8 mm length and 0.15 mm wall thickness. Initial experiments showed that the corundum and quartz crystals were mechanically coherent, obviating the need for containment of the crystals in an inner capsule, as was done in some previous solubility studies using otherwise similar methods (e.g., wollastonite, Newton and Manning, 2006, 2007). Materials were loaded into the tube segments in the order crystals, H_2O, NaCl, with weighings on a Mettler M3 microbalance at each step ($1\sigma=2$ μg).

All experiments were conducted in a piston-cylinder apparatus (3/4-inch diameter) with NaCl pressure medium and graphite heater sleeve. Approach to run conditions, monitoring of *P* and *T*, and quench procedures were as described by Newton and Manning (2000, 2006). Experimental pressure and temperature are considered accurate to ±300 bars and ±3 °C.

After quenching, H_2O contents were checked by drying punctured capsules; H_2O lost during drying (H_2O out) agreed with H_2O initially added (H_2O in) to within 0.6 wt.% (Table 1), except in a few cases where fluid sprayed out upon puncturing, with some loss of NaCl along with the H_2O. All solution compositions were calculated using the H_2O-in value. NaCl mole fraction (X_{NaCl}) was calculated from $X_{NaCl}=n_{NaCl}/(n_{NaCl}+n_{H_2O})$, where *n* is the number of moles of the subscripted component; that is, X_{NaCl} values neglect dissolved Al_2O_3 and SiO_2. Acid–base relations of selected quenched fluids were characterized approximately using pH paper, as described in Newton and Manning (2006).

Corundum solubilities (Table 1) were determined by weight losses of crystals retrieved from quenched capsules. Uncertainties in concentrations are based on propagated weighing uncertainties. Interpretation of run products was based on examination of quenched and dried experimental charges, optical microscopy and electron-beam microscopy and microanalysis.

3. Results

3.1. Characterization of run products

In most cases, the nature of the run products was evident at a glance using a binocular optical microscope at low magnification. All dried charges from NaCl-bearing runs contained large amounts of quenched halite. This was removed by rinsing with H_2O to study textures of the other phases. Residual corundum and, in a few experiments, quartz crystals displayed new crystal faces, arrays of etch pits, and solution-rounded portions. The crystal surfaces were quite clean, except in runs where melt was inferred to have formed (see below).

Most experiments were in the quartz-undersaturated region, and the quartz added to the charge completely dissolved during the run. In runs at $X_{NaCl} \leq 0.03$ with the highest bulk SiO_2 content (Table 1), residual quartz was present as a single subhedral crystal or small neoblasts, indicating quartz saturation. The assemblage corundum+quartz is slightly metastable relative to kyanite+quartz at 800 °C and 10 kbar (Harlov and Newton, 1993). The possible presence of kyanite or sillimanite was carefully checked by thorough examination of the capsule walls at high magnification, and by characterization of the quench material with X-ray diffraction (Norelco diffractometer, monochromatic Cu Kα radiation, 1° 2θ/min scans) and optical microscopy in oil immersion mounts. Selected run products were also examined by scanning-electron microscopy, and in several cases analyzed using energy-dispersive spectroscopy (Leo 1430VP, 15 kV, 1 μm spot size). No evidence for the appearance of aluminum silicates was ever found.

Relatively large glass spheres appeared instead of quartz in runs with the highest bulk SiO_2 contents at $X_{NaCl} > 0.03$ (Table 1). The spheres were much larger and compositionally distinct from the ubiquitous "fish roe", which represents quenched

Table 1
Results of experiments on corundum+SiO_2+H_2O+NaCl

Experiment no.	Time (h)	H_2O in (mg)	H_2O out (mg)	NaCl in (mg)	X_{NaCl}	Cor in (mg)	Cor out (mg)	Qz in (mg)	Qz out (mg)	$m_{Al_2O_3}$ (×10^3)	m_{Si}	Quench pH	Notes
Si-19	24	36.562	36.214	0	0	2.761	2.746	1.735	0	4.0(8)	0.790(1)		
Si-18	21	37.605	37.762	0	0	1.959	1.936	2.539	0	6.0(7)	1.124(1)		
Si-42	90	38.078	–	0	0	5.694	5.671	2.848	0	5.9(7)	1.245(1)	5–6	
Si-21	24	36.817	–	0	0	2.747	2.723	5.347	2.557	6.4(8)	1.261(1)	5–6	Q1
Si-15	20	35.835	35.746	0.559	0.005	2.811	2.792	0.696	0	5.2(8)	0.323(1)		
Si-17	24	36.282	36.178	0.547	0.005	2.790	2.762	1.501	0	7.6(8)	0.689(1)		
Si-16	22	35.463	36.131	0.774	0.007	2.011	1.959	2.390	0	14.4(8)	1.122(1)		
Si-23	15	36.180	–	0.527	0.004	6.054	5.998	3.824	>0.930	15.2(8)	<1.331(1)	2	Q2
Si-13	24	37.197	37.061	3.602	0.029	2.864	2.811	1.344	0	14.0(7)	0.604(1)		
Si-14	20	36.633	36.868	3.412	0.028	2.102	2.013	2.195	0	23.8(8)	0.991(1)		
Si-26	20	36.489	–	3.266	0.027	5.747	5.631	2.812	0	31.2(8)	1.283(1)	1	
Si-36	72	34.417	34.276	3.470	0.030	5.964	5.861	2.917	–	29.4(8)	<1.411(1)		Q3
Si-48	22	36.805	–	3.433	0.028	4.498	4.383	3.856	0.593	30.6(8)	1.476(1)		Q1,S
Si-12	20	30.950	–	11.381	0.102	2.913	2.859	0.751	0	17.1(9)	0.404(2)		S
Si-11	19	31.489	31.360	11.673	0.103	2.193	2.100	1.506	0	29.0(9)	0.796(1)		
Si-24	23	34.692	–	12.148	0.097	5.999	5.885	1.868	0	32.2(8)	0.896(1)	1	
Si-50	161	31.976	31.754	11.522	0.100	4.380	4.261	1.919	0	36.5(9)	0.999(1)		
Si-25	22	36.614	–	13.285	0.101	5.884	5.746	2.229	0	37.0(8)	1.013(1)	1	
Si-41	71	36.712	–	12.870	0.098	4.881	4.740	2.273	0	37.7(8)	1.030(1)	1	
Si-46	66	30.074	–	10.591	0.098	5.651	5.538	1.932	0	<36.9(9)	<1.069(2)		M1,S
Si-49	94	37.217	–	13.313	0.099	3.863	3.719	2.411	0	<37.9(7)	<1.078(1)		A,S
Si-27	20	36.605	36.540	13.144	0.100	5.631	–	2.397	0	–	<1.090(1)		A,M2
Si-43	96	37.075	36.875	13.242	0.099	4.746	4.595	2.546	0	<39.9(8)	<1.143(1)		A,M1
Si-31	20	25.219	25.062	20.144	0.198	5.108	–	1.137	–	–	–		M2
Si-20	22	30.707	30.446	24.552	0.198	4.191	–	3.076	–	–	–		A,M2,Q2
Si-8	23	24.608	24.496	33.294	0.295	2.298	2.258	0.238	0	15.9(11)	0.161(1)		
Si-39	68	30.765	30.853	42.796	0.300	5.766	5.694	0.512	0	23.0(9)	0.277(1)		
Si-4	27	25.450	24.849	35.411	0.305	2.348	2.298	0.451	0	19.3(11)	0.295(1)		
Si-9	17	25.778	25.651	35.357	0.298	1.937	1.882	0.576	0	20.9(11)	0.372(1)		
Si-37	74	30.390	–	41.896	0.298	5.860	5.770	0.785	0	29.0(9)	0.430(2)	1	
Si-10	21	24.792	24.572	33.800	0.298	2.257	2.191	0.716	0	26.1(11)	0.481(1)		
Si-45	167	27.337	27.223	37.788	0.299	4.594	4.496	0.900	0	35.2(10)	0.548(1)		
Si-38	67	30.806	30.688	42.953	0.301	3.956	3.820	1.143	0	43.3(9)	0.618(1)		
Si-51	86	31.096	30.965	43.704	0.302	3.720	3.579	1.208	0	44.5(9)	0.647(2)		
Si-53	159	29.057	28.810	40.685	0.301	0.873	0.737	1.222	0	45.9(10)	0.700(2)		
Si-54	159	28.827	28.834	40.140	0.300	1.932	1.793	1.971	0	<47.3(10)	<1.138(2)		A,M1
Si-40	95	29.144	29.104	42.773	0.311	3.819	–	1.181	0	–	<0.674(2)		A,M2
Si-52	162	16.912	16.938	55.193	0.501	32.616	32.554	0.384	0	36.0(16)	0.378(3)		

Explanation. "In" and "out" respectively refer to weights before and after experiment; H_2O-in used to determine X_{NaCl} and solubilities. Qz, quartz; Cor, corundum; $m_{Al_2O_3}$, Al_2O_3 molality (multiplied by 10^3); m_{Si}, Si molality. Dashes indicate that measurement could not be made or was unreliable. Parenthetical numbers following solubilities indicate propagated weighing error, expressed as 1σ uncertainty in last significant digit(s). Abbreviations under "Notes": Q indicates quartz present (Q1, single, clean quartz crystal; Q2, single crystal and unweighable, small quartz neoblasts; Q3, unweighable small quartz neoblasts only; Q2 and Q3 runs give maximum m_{Si} only); M indicates melt present (M1, quenched melt spheres, all solubilities are maxima; M2, quenched melt spheres and coatings on quartz and/or corundum, which preclude solubility determination for coated phase; see text); A, albite present (unweighable), all solubilities maxima; S, capsule sprayed fluid on opening.

solutes (Fig. 1a; Table 2). The glass spheres are interpreted to be quenched siliceous melt: their compositions on an anhydrous basis are nearly on the join $NaAlSi_3O_8$–SiO_2 (Table 2). In charges with melt spheres, the corundum commonly had a glassy coating adhering to the surface (Fig. 1b). In runs of short duration at high salinity, residual quartz crystals were also coated with glass (Si-20, Table 1). This is interpreted to result from metastable melting because quartz was not observed to coexist with glass in runs of at least 3 days duration (see below). Compositional analyses (Table 2) showed that the coating has the same composition as the glass spheres. The coatings rendered weight changes indeterminate. Albite appeared in almost every run that yielded glass spheres. In runs at X_{NaCl}=0.1, the albite occurred as disseminated crystals of 25–50 μm size; in runs at $X_{NaCl} \geq 0.2$, the high-SiO_2 runs yielded radiating clusters of albite perched on residual corundum crystals (Fig. 1c, d). Quartz was not observed to coexist with either glass spheres or albite. Thus, corundum solubility is limited at high X_{NaCl} and high SiO_2 by saturation with albite+melt, rather than by quartz. This change in phase assemblages takes place between X_{NaCl}=0.03 and 0.10 (Table 1).

A few trial experiments on kyanite instead of corundum at the same P–T and X_{NaCl}=0.3 were unsuccessful in defining Al_2O_3 solubility, because of the formation of secondary corundum at low SiO_2 concentrations. In fluids with high SiO_2 and high NaCl, a tightly adhering crust of small albite crystals formed which could not be removed from the kyanite, compromising the weighing. No glassy coatings or melt spheres were found in these experimental charges. These experiments are not listed in Table 1.

3.2. Attainment of equilibrium

Tropper and Manning (2007) found that run durations of 12 h were sufficient for attainment of equilibrium in the system corundum–H_2O. However, it is possible that dissolution rates are slower in fluids rich in SiO_2, Al_2O_3 and NaCl, where polymerized species could lower diffusive and/or advective transport in the charge. We evaluated the approach to equilibrium at X_{NaCl} values of 0.1 and 0.3. At the lower X_{NaCl}, three experiments were conducted at m_{Si}=1.0 for 22, 71 and 161 h (Si-25, 41 and 50, respectively; Table 1). The results show no detectable difference in Al content, and it was assumed, following Tropper and Manning (2007), that 15–24 h runs were sufficient to attain equilibrium at $X_{NaCl} \leq 0.1$. However, at X_{NaCl}=0.3, experimental durations of one day

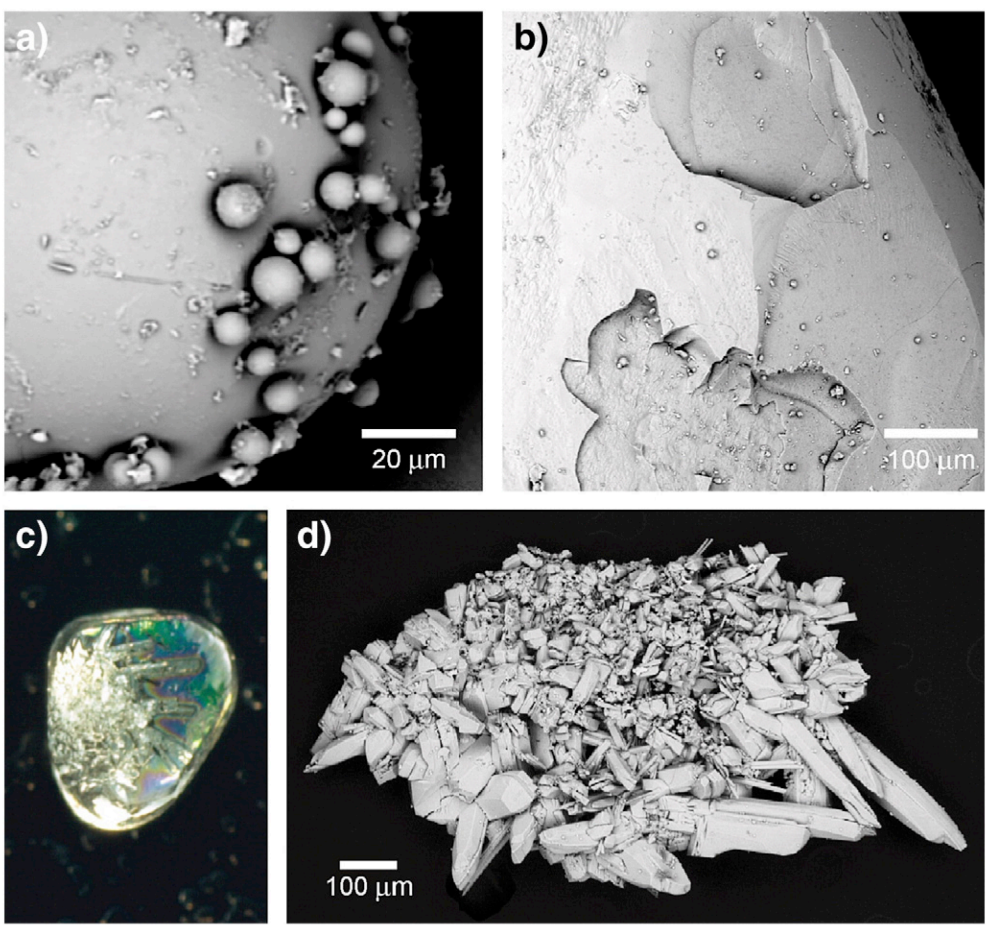

Fig. 1. (a) Back-scattered electron (BSE) image of quenched melt sphere from Al_2O_3-saturated experiment at X_{NaCl}=0.2 (Run Si-31, Table 1). The smaller spheres ("roe") perched on the larger sphere are quench-precipitates from the fluid phase. They are considerably more silica-rich than the melt sphere. (b) BSE image of aluminosilicate glass coat on surface of corundum crystal, partly broken away (Run Si-31, Table 1). (c). Optical plane-light image of corundum crystal showing impression of cluster of albite crystals which grew on surface. Crystal is ~1 mm in longest dimension. The original position of the crystals shows that they were grown from an metastable glassy coating which subsequently devitrified (Run Si-40, Table 1). (d) The cluster of albite crystals grown on corundum surface in (c).

Table 2
Energy dispersive analyses of quenched melt and vapor

	Albite (theoretical)	Albite glass (synthetic)			Si-31 melt spheres			Si-20 glassy coating on Qz			Si-20 glassy coating on Cor	Si-31 roe	
		1	2	3	1	2	3	1	2	3	1	1	2
SiO_2	68.74	67.19	67.79	66.66	78.95	77.58	80.46	76.20	78.37	78.84	80.65	89.26	91.43
Al_2O_3	19.44	21.47	21.36	21.54	13.33	13.71	13.21	15.56	13.43	13.12	15.06	5.84	3.53
Na_2O	11.82	11.12	11.59	11.42	6.55	7.64	5.49	7.78	7.26	6.64	3.09	1.72	1.71
Cl_2O	0	0.23	0.26	0.38	1.17	1.07	0.84	0.46	0.94	0.80	1.20	2.78	3.06

All analyses normalized to 100 wt%. Three different Si-31 melt spheres analyzed. “Roe” refers to vapor-quench precipitate. Synthetic albite glass used as a standard; apparent presence of Cl indicates that concentrations of this element are somewhat uncertain.

proved to be too short (Table 1). For example, run Si-4 (27 h) gave lower dissolved Al than run Si-39 (68 h), despite higher SiO_2 content in the former. A similar apparent inconsistency occurred for experiments Si-10 and Si-37. In contrast, there is no evident time-dependent solubility difference among runs of more than ~3 days duration. Thus, runs of at least ~3 days are required to attain equilibrium in the more concentrated solutions, and the experiments with shorter run durations of 17–27 h at $X_{NaCl}=0.2$–0.3 were assumed to have failed to reach equilibrium (Table 1).

Quartz dissolution is very rapid at the experimental conditions: H_2O–SiO_2 fluid equilibration takes place in less than 2 h at 700 °C and 10 kbar pressure (Newton and Manning, 2003). Thus, it was assumed that the run times were sufficient for equilibration within the fluid-SiO_2 subsystem.

3.3. Corundum solubility

Experimental results are presented in Table 1 and Figs. 2 and 3. In the compositional region where the two-phase assemblage corundum + fluid is stable, corundum solubility increases with increasing SiO_2 and NaCl concentrations. If only one of these components is present, the effect is minor; however, addition of both NaCl and SiO_2 leads to a strong increase in corundum solubility (Figs. 2 and 3). Thus, SiO_2 and NaCl together enhance the solubility of corundum to an extent greater than either component alone.

The presence of quartz or albite + melt at the highest SiO_2 concentrations defines the upper limit of corundum solubility at 800 °C, 10 kbar, in the system Al_2O_3–SiO_2–NaCl–H_2O. At $X_{NaCl} \leq 0.03$, where the additional phase was quartz, the weight

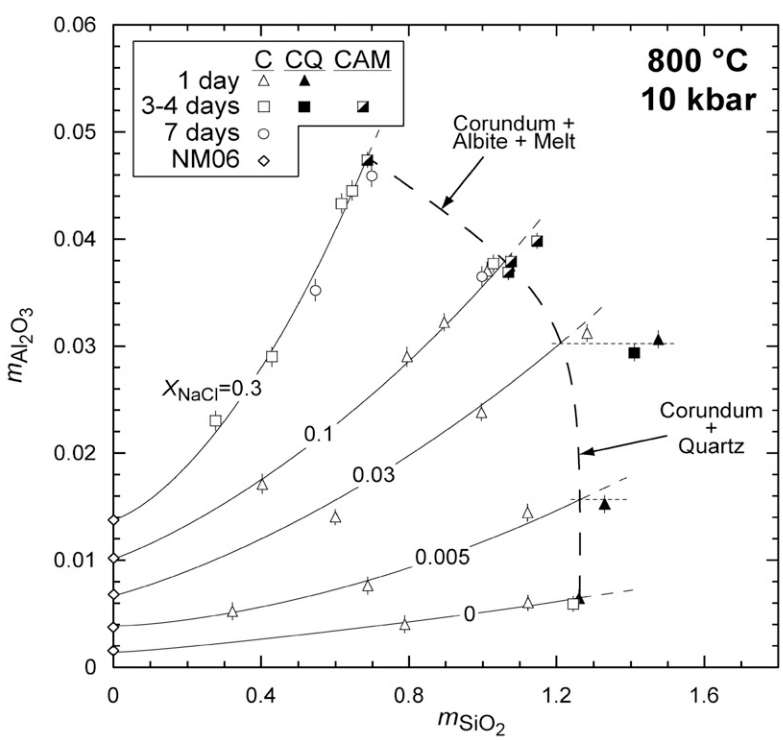

Fig. 2. Experimental data on corundum solubility in H_2O–NaCl fluids as a function of SiO_2 molality. Data in SiO_2-free fluids (open diamonds) from Newton and Manning (2006; NM06). Other data from the present work, including fluid composition in presence of corundum only (“C,” open symbols), corundum + quartz (“CQ,” filled symbols) and corundum + albite + melt (“CAM,” half-filled squares). NaCl contours (solid lines) are from Eqs. (1A) and (1B), text. Quartz–corundum saturation at $X_{NaCl} \leq 0.03$ (metastable with respect to kyanite + quartz) and saturation with albite + melt at higher salinities are shown with the long-dashed line. Quartz saturation determined by constant Al_2O_3 solubility above a threshold SiO_2 concentration (dotted lines). At $X_{NaCl}=0.3$, one-day runs (Table 1) were insufficient for equilibrium (see text) and are not shown; the Ab + L datum was derived by combining results from runs Si-40 and Si-54 (Table 1).

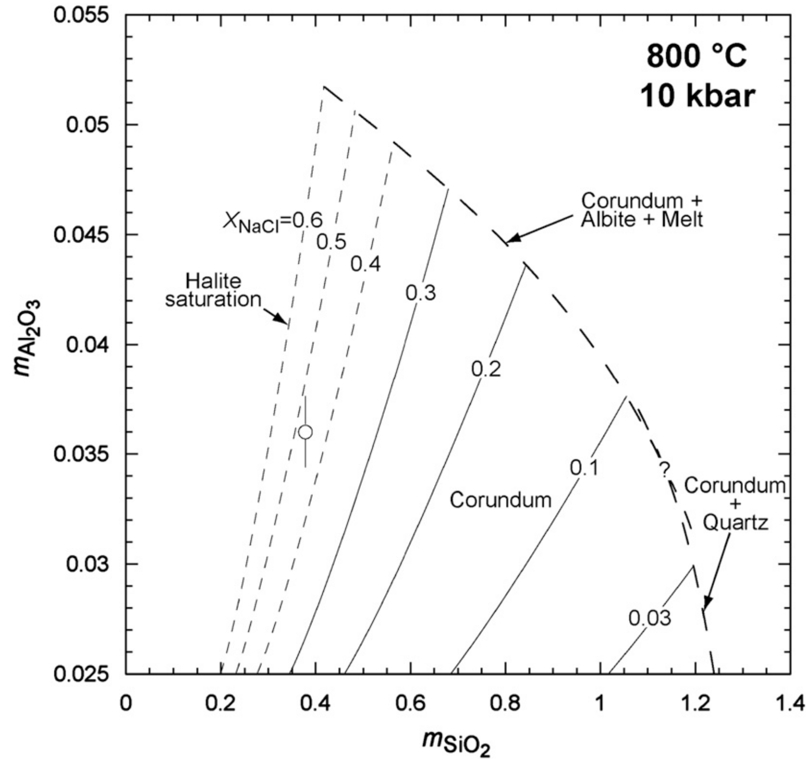

Fig. 3. Interpreted phase relations of corundum, quartz, albite, melt and fluid in the system Al_2O_3–SiO_2–H_2O–NaCl at 800 °C and 10 kbar, based on the present experiments. Solid lines denote X_{NaCl} isopleths calculated from Eq. (1B) (short dashed where extrapolated). The single result for corundum solubility at $X_{NaCl}=0.5$ is shown for comparison with extrapolated isopleths. Long dashed lines show inferred saturation envelopes for corundum+quartz and corundum+albite+melt, which intersect at an invariant point (queried) that must lie between $X_{NaCl}=0.03$ and 0.10. The corundum+quartz envelope is metastable with respect to kyanite+quartz.

change of the residual quartz crystal could be determined only in run Si-21 at $X_{NaCl}=0$ (Table 1). This experiment permitted direct determination of $m_{Si}=1.261$ at quartz saturation in the NaCl-free system. At $X_{NaCl}=0.005$, minute, unweighable quartz crystals were present in addition to the single grain; the weight change of the initial quartz grain therefore provides only a maximum limit. The same problem and disequilibrium likely affected quartz-saturated runs at $X_{NaCl}=0.03$. In run Si-48 (22 h), the weight change of the quartz crystal yielded $m_{Si}=1.476$; however, a longer experiment (Si-36, 72 h), which produced minute, unweighable quartz crystals, limits quartz saturation to no greater than $m_{Si}=1.411$, assuming complete dissolution of the original crystal. It is possible that the inconsistency results from the undetected presence of quartz neoblasts in run Si-48.

Inferred concentrations in the presence of albite and liquid at $X_{NaCl}>0.03$ constrain the location of the corundum+albite+melt-saturation envelope. At $X_{NaCl}=0.10$, experiments in which albite and/or melt were present provide an upper limit to the saturation surface (Fig. 2). Coatings on grains prevented determinations of even maximum limits at $X_{NaCl}=0.2$. However two experiments with albite+melt (Table 1) can be combined to give a relatively tight upper limit on the saturation surface at $X_{NaCl}=0.3$ (Fig. 2). Taken together, the data indicate that saturation with albite+melt at $X_{NaCl}>0.03$ occurs at lower SiO_2 concentration than saturation with quartz at $X_{NaCl}\leq 0.03$.

4. Discussion

4.1. Corundum solubility and phase relations in the system Al_2O_3–SiO_2–H_2O–NaCl

The experiments demonstrate that corundum solubility increases due to the presence of SiO_2 and NaCl in H_2O at 800 °C, 10 kbar. The solubility data in the quartz-undersaturated region (Figs. 2, 3) can be described accurately by quadratic expressions in X_{NaCl} and $\sqrt{X_{NaCl}}$, if dilute and concentrated salinity regions are treated separately. Least-squares fitting to the data yielded Al_2O_3 molality ($m_{Al_2O_3}$) at corundum saturation given by

$$m_{Al_2O_3} = m^{\circ}_{Al_2O_3} + \left(0.0025 - 0.0487X_{NaCl} + 9.733X^2_{NaCl}\right)m_{SiO_2} + \left(0.0012 - 0.210X_{NaCl} + 0.0757X^{1/2}_{NaCl}\right)m^2_{SiO_2} \tag{1A}$$

for $0 \leq X_{NaCl} \leq 0.03$, and, for $X_{NaCl}>0.03$,

$$m_{Al_2O_3} = m^{\circ}_{Al_2O_3} + \left(0.0038 - 0.033X_{NaCl} + 0.0406X^{1/2}_{NaCl}\right)m_{SiO_2} + \left(0.0076 - 0.0006X_{NaCl} + 0.455X^2_{NaCl}\right)m^2_{SiO_2} \tag{1B}$$

where $m^{\circ}_{Al_2O_3}$ is the Al_2O_3 molality in the SiO_2-free system at 800 °C, 10 kbar and the same X_{NaCl}, as determined from Eq. (3) of Newton and Manning (2006). The NaCl isopleths calculated from Eqs. (1A) and (1B) are plotted in Figs. 2 and 3.

The locations of the quartz or albite + melt-saturation envelopes (Figs. 2, 3) were derived based on the following considerations. At $X_{NaCl} \leq 0.03$, the observed presence of residual quartz requires that the Al_2O_3 content, as well as the SiO_2 content, of the fluid become invariant. Accordingly, the intersection of a horizontal line through the nominal m_{Si} values (based on the bulk compositions of the charges) with the empirical SiO_2-undersaturated NaCl isopleths of m_{Al_2O3} yields a point on the quartz-saturation envelope, though uncertainty grows with increasing extrapolation. Quartz was not actually verified in one experiment at $X_{NaCl} = 0.03$, interpreted to be only just quartz saturated (Si-26, Table 1), but roughly constant Al_2O_3 molality values with increasing SiO_2 suggest that quartz saturation was attained. When the assemblage albite + melt replaces quartz to limit SiO_2 increase in the fluid, the position of the envelope is bracketed by the bulk compositions of experiments either containing or lacking this assemblage. The corundum + quartz and corundum + albite + melt-saturation envelopes must intersect at an invariant point that is only broadly constrained to lie between $X_{NaCl} = 0.03$ and 0.10 (schematically shown in Fig. 3).

The fitted X_{NaCl} isopleths in Figs. 2 and 3 illustrate that, at a fixed SiO_2 concentration, m_{Al_2O3} rises steeply with NaCl concentration up to $X_{NaCl} = 0.03$. At higher X_{NaCl}, it increases more slowly with increasing salinity, to a maximum near 0.05 molal at halite saturation.

4.2. Aluminum silicate solubility

Solubilities of kyanite and sillimanite at 800 °C and 10 kbar can be inferred from the present data to a good approximation, since their Gibbs free energies of formation from the oxides at these conditions are well known and quite small. The reaction

$$\underset{\text{corundum}}{Al_2O_3} + \underset{\text{quartz}}{SiO_2} = \underset{\text{kyanite}}{Al_2SiO_5} \tag{2}$$

has a Gibbs free energy change of −1080 J at 800 °C and 10 kbar (Holland and Powell, 1998). This small negative quantity requires that the solubility of kyanite in the system Al_2O_3–SiO_2–H_2O–NaCl at 800 °C and 10 kbar should be only a few percent lower than that of corundum + quartz at the same conditions. Since kyanite–sillimanite equilibrium almost exactly coincides with these P–T conditions (Bohlen et al., 1991), this conclusion applies equally well to sillimanite. Thus, the Al_2O_3 saturation envelope of Figs. 2 and 3 gives, to a good approximation, the Al_2O_3 molality of NaCl–H_2O fluids

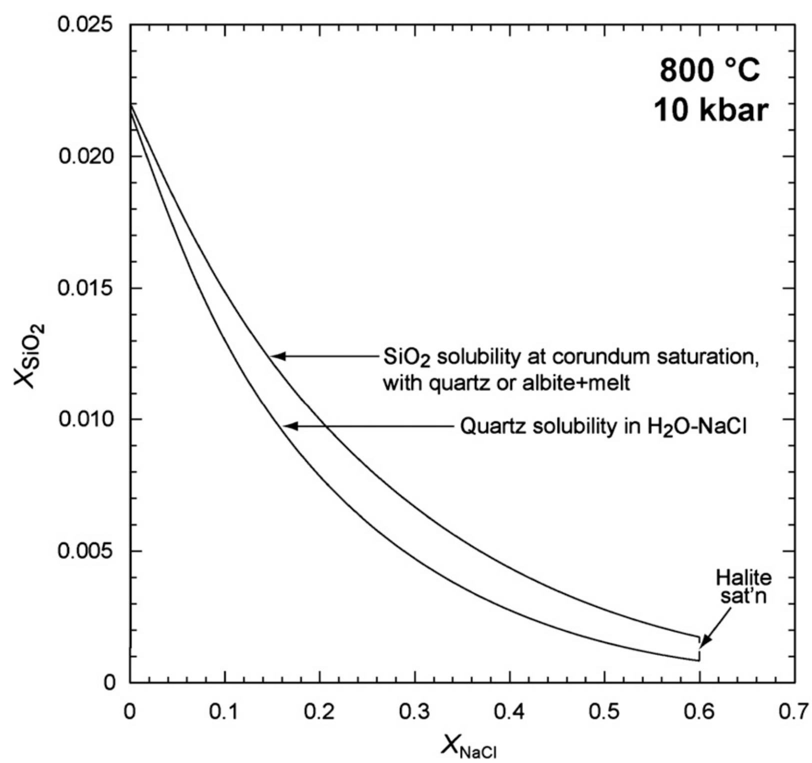

Fig. 4. Estimated SiO_2 saturation molality in the presence of corundum and NaCl at 800 °C, 10 kbar. The curves are fits to data of Newton and Manning (2000) on quartz solubility in H_2O–NaCl ($m_{SiO_2} = 1.231\exp(-3.098X_{NaCl})$; $R^2 = 0.998$) and quartz or albite + melt saturation in the presence of corundum ($m_{SiO_2} = 1.247\exp(-1.944X_{NaCl})$; $R^2 = 0.997$), converted to mole fraction using $X_i = m_i/m_i + 55.51(1 + 2X_{NaCl}/[1 - X_{NaCl}])$, where the factor 2 arises from the assumption of full dissociation of NaCl at these conditions (Aranovich and Newton, 1996; see text). The corundum-saturated SiO_2 solubility envelope omits the poorly constrained invariant point between marking the intersection of the quartz-saturation and of albite + melt-saturation surfaces. The difference in solute SiO_2 between the curves is interpreted to be the result of enhancement by Na–Al, Al–Si, and/or possible Na–Al–Si complexing (see text).

coexisting with aluminum silicate and quartz at 800 °C and 10 kbar.

4.3. Reciprocal enhancement of Al_2O_3 and SiO_2 solubility in H_2O–NaCl fluids

When combined with the results of Newton and Manning (2006), the present study shows that where corundum + quartz or corundum + albite + melt coexist with an H_2O–NaCl fluid, dissolved Al_2O_3 and SiO_2 concentrations are higher at a given X_{NaCl} than when corundum or quartz is present alone. The extent of this reciprocal enhancement of Al_2O_3 and SiO_2 changes with X_{NaCl}.

The effect of Al_2O_3 on SiO_2 solubility with varying NaCl is shown in Fig. 4. Newton and Manning (2000, 2006) found that quartz solubility in H_2O–NaCl at 800 °C, 10 kbar, decreases exponentially with increasing X_{NaCl}. Their results are shown in Fig. 4 as SiO_2 mole fraction (X_{SiO_2}) assuming fully dissociated NaCl. This choice of speciation is consistent with activity measurements in NaCl–H_2O mixtures at high P and T by Aranovich and Newton (1996) and with deductions from quartz solubility in NaCl–H_2O given by Newton and Manning (2006). Values of X_{SiO_2} in the presence of corundum at quartz or albite + melt saturation were derived from Figs. 2 and 3 and fit to a smooth exponential function. The resulting curve illustrates that dissolved SiO_2 is enhanced to an increasing degree with added NaCl in the presence of corundum, relative to the Al_2O_3-free system SiO_2–H_2O–NaCl. The extent of enhancement reaches ~100% at halite saturation.

The effect of SiO_2 on Al_2O_3 in H_2O–NaCl fluids is shown in Fig. 5. Al_2O_3 and SiO_2 mole fractions are again calculated with respect to completely dissociated NaCl (Newton and Manning, 2006). Enhancement of Al_2O_3 solubility by NaCl alone occurs in the low-salinity range, with a maximum at X_{NaCl}~0.1. Isopleths of X_{SiO_2} show that addition of SiO_2 to the fluid promotes further Al_2O_3 dissolution and that the maximum in corundum solubility along SiO_2 isopleths disappears. However, the saturation envelope depicting coexistence of corundum + fluid with quartz or albite + corundum, along which X_{SiO_2} is variable, rises with increasing NaCl to a maximum at X_{NaCl}~0.08–0.10, at which $X_{Al_2O_3}$ is ~25 times greater than corundum solubility in pure H_2O. A maximum in the saturation envelope occurs in this plot, but not in Figs. 2 and 3, because of the use of the molality scale in those figures.

4.4. Origin of reciprocal solubility enhancement

The present experiments place three constraints on the mechanism that drives the reciprocal enhancement of Al_2O_3 and SiO_2 solubility. The first is that, in the NaCl-free experiments (Fig. 2), corundum solubility increases with the addition of SiO_2 to H_2O. Manning (2007) showed that, at similar conditions of 700 °C, 10 kbar, the enhancement of Al_2O_3 solubility by dissolved SiO_2 is best explained by formation of polymeric Si–

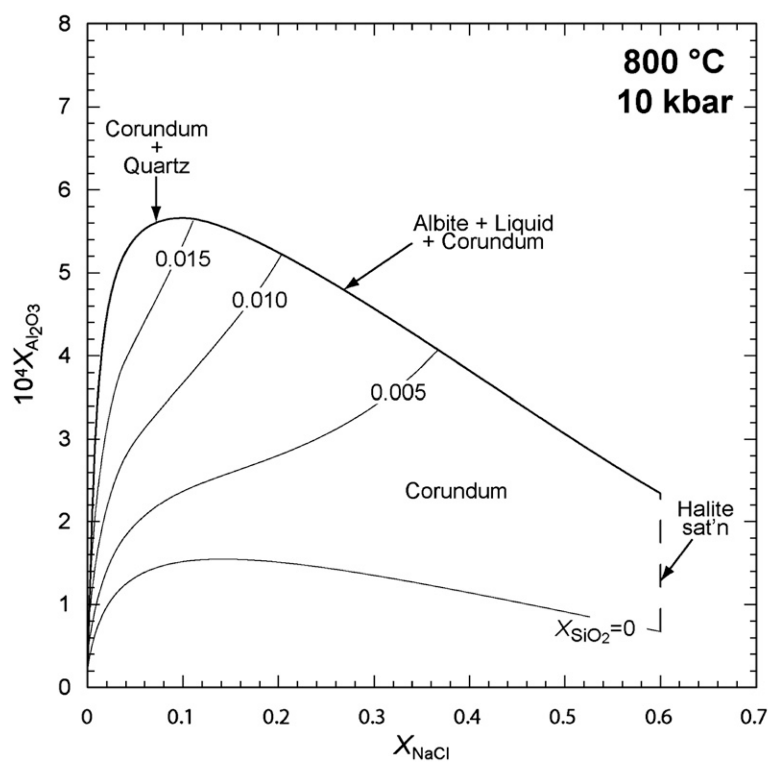

Fig. 5. Al_2O_3 solubility in silica-bearing NaCl solutions at 800 °C and 10 kbar, plotted in terms of mole fraction. Mole fractions are calculated with respect to completely dissociated NaCl (see Fig. 4, caption). The SiO_2 isopleths are calculated from Eq. (1A) and (1B), text. The corundum-saturated SiO_2 saturation envelope omits the poorly constrained invariant point between marking the intersection of the quartz-saturation and of albite + melt-saturation surfaces. Noteworthy is the very large enhancement of Al_2O_3 solubility in the range $0 \le X_{NaCl} \le 0.1$. NaCl concentration of 20–25 wt.% near the maximum in the saturation envelope will yield the greatest Al_2O_3 solubility at deep-crustal conditions, in the quaternary system Al_2O_3–SiO_2–H_2O–NaCl.

Al complexes. The formation of such species at high P and T is supported by independent evidence for aqueous silica dimers and higher-order multimers (Zotov and Keppler, 2000, 2002; Newton and Manning, 2002, 2003) and Na–Al species in $H_2O\pm NaCl$ (Anderson and Burnham, 1983; Newton and Manning, 2006) at high P and T.

A second constraint on the mechanism of reciprocal solubility enhancement is the fluid composition along the quartz/albite+melt-saturation envelopes, where Al and Si concentrations are greater than with corundum or quartz alone in H_2O–NaCl at a given salinity. This effect can be assessed using the excess solute Si/Al ratio, A_{ex}, as calculated from

$$A_{ex} = \frac{m_{SiO_2} - \overset{\circ}{m}_{SiO_2}}{2\left(m_{Al_2O_3} - \overset{\circ}{m}_{Al_2O_3}\right)} \tag{3}$$

where m_i are molalities of the subscripted compounds in the quaternary system SiO_2–Al_2O_3–H_2O–NaCl, $\overset{\circ}{m}_{SiO_2}$ represents SiO_2 molality at quartz saturation in the ternary system SiO_2–NaCl–H_2O (Newton and Manning, 2000, 2006), and $\overset{\circ}{m}_{Al_2O_3}$ is Al_2O_3 molality at corundum saturation in the ternary system Al_2O_3–NaCl–H_2O (Newton and Manning, 2006). The parameter A_{ex} was estimated by determining $m_{Al_2O_3}$and m_{SiO_2} at the intersections of solubility isopleths (Eqs. 1A and 1B) with the quartz or albite+melt-saturation boundaries (Figs. 2 and 3). Inferred values of A_{ex} (Table 3) increase with increasing X_{NaCl}. At low X_{NaCl} the uncertainty in A_{ex} is large; for $X_{NaCl}=0$, the value could lie anywhere between 1 and 2. The value of A_{ex} increases rapidly to 2.5 at $X_{NaCl}=0.1$, and then rises more slowly to >3.0 at higher salinities.

The third constraint on the mechanism of reciprocal solubility enhancement comes from the quench pH of the experimental fluids and the composition of quench roe. In the absence of NaCl (Table 1) or SiO_2 (Newton and Manning, 2006), quench pH was neutral to slightly acidic; however, strongly acidic pH of 1–2 was recorded in quenched fluids over a range of X_{NaCl} and m_{Si} (Table 1). The very low quench pH suggests that H^+ was produced to balance a large anion excess, which indicates high Cl^- relative to Na^+ because these are the dominant solutes. The high H^+ activity in the quench fluids could reflect a combination of the following processes: the (unknown) net charge of solute complexes in the fluid at 800 °C and 10 kbar will cause consumption or production of H^+ to give an equilibrium pH at high P and T; melt, if present, may shift pH at high P and T; and upon quenching of the experiment, precipitation from the fluid (e.g., quench roe) removes solutes and causes pH adjustment. (Halite precipitation at room P and T prior to capsule opening removes both Na and Cl from the experimental solution but does not affect pH, so it can be neglected.)

Table 3
Molar excess Si/Al ratios (A_{ex}) in fluids along the quartz- and albite+melt-saturation envelope at 800 °C and 10 kbar

X_{NaCl}	$m_{Al_2O_3}$	$\overset{\circ}{m}_{Al_2O_3}$	m_{SiO_2}	$\overset{\circ}{m}_{SiO_2}$	A_{ex}
0	0.0064	0.0014	1.26	1.25	1–2
0.005	0.015	0.0037	1.25	1.23	1–2
0.03	0.030	0.0062	1.20	1.14	1–2
0.10	0.038	0.010	1.05	0.91	2.5
0.30	0.047	0.014	0.72	0.49	3.5
0.50	0.051	0.015	0.49	0.26	3.2

Explanation: m_i is molality of subscripted component; $\overset{\circ}{m}_i$ refers to molality in the subsystem i–H_2O–NaCl. Values of A_{ex} at $X_{NaCl}\leq 0.03$ are given as a range because uncertainty in m_{SiO_2} translates to wide range in A_{ex}.

Quench precipitation is unlikely to lead to the very low observed pH because analyses of the roe indicate Cl>Na (Table 2). Formation of quench roe should therefore act as a neutralizing agent rather than an agent of acidification. This can be appreciated by model speciation calculations at 25 °C (Geochemist's Workbench, Bethke, 1996, with the LLNL database of Delany and Lundeen, 1989). The calculations are necessarily approximate: they assume an equilibrium distribution of species at 25 °C; the database includes multimeric complexes of Al and Si, and NaH_3SiO_4, but there are no data for more complex polymers which may form or be metastably inherited from high P and T; and calculated ionic strengths of ~6 limit the accuracy of the B-dot model for activity coefficients. Nevertheless, a first-order appreciation of the effect of preferential removal of Cl in excess of Na can be gained by this approach. Assuming conditions of $X_{NaCl}=0.1$ and corundum+albite+melt saturation, Al and Si molalities before quenching are respectively 0.076 and 1.040 (Table 1). Upon quenching to 25 °C, the fluid is supersaturated with respect to halite, other minerals and quench roe. After adjusting the fluid to halite saturation and suppressing precipitation of other minerals, fluid pH is 5.0. Progressive removal of Na, Al, Si and Cl in proportions corresponding to the composition of quench roe causes pH to increase to >7. Similar effects would be seen at other NaCl concentrations, assuming the composition of quench roe is constant. The magnitude of the pH adjustment for a given aliquot of quench roe removed will vary depending on additional species included and use of different activity coefficients; however, the shift to higher pH values would be preserved. Thus, the calculations illustrate that removal of more Cl than Na by the quench material leads to an increase in the pH of the solution and, given our assumptions, would not generate the low pH observed. This suggests that the acid pH of the quench fluid is inherited from high P and T.

The three constraints discussed above – Si–Al polymerization, variation in A_{ex} with X_{NaCl}, and acidic quench pH – support the hypothesis that reciprocal Al and Si solubility enhancement is caused by polymeric species involving combinations of Al, Si, and Na which partition Na more strongly than Cl. This in turn produces HCl, which dissociates on quenching to give the observed low pH at room P and T. The simplest approach is to consider the coexistence of separate Na–Al complexes and Al–Si complexes, as identified by Newton and Manning (2006) and Manning (2007), respectively. Assuming Na/Al=1 and neutral complexes, a model dissolution reaction would be:

$$\underset{\text{corundum}}{Al_2O_3} + NaCl + A_{ex}Si(OH)_4 = NaAlO_{(4-B)/2}(OH)_B + AlSi_{A_{ex}}O_{(3+4A_{ex}-C)/2}(OH)_C + (4A_{ex} - B - C - 1)/2\ H_2O + HCl \tag{4}$$

where A_{ex} is from Eq. (3) and B and C are the hydration states of the Na–Al and Al–Si complexes, respectively.

Anderson and Burnham (1983) suggested that an albite-like Na–Al–Si complex might be important in explaining observed high Al solubility in H_2O resulting from nearly congruent albite solubility at high P and T. Possible evidence in favor of this hypothesis as it applies to an NaCl-rich solvent might be found in the fact that the inferred total Si/Al ratio of the solutes is near 3 for the highest Al concentrations (and salinity) and the fact that crystalline albite is an Al-saturation product at these conditions. The bulk composition of polymerized species can be linked to interaction of excess dissolved Al_2O_3, $Si(OH)_4$ and NaCl via the mass balance relation

$$\underset{\text{corundum}}{Al_2O_3} + 2NaCl + 2A_{ex}Si(OH)_4 = 2NaAlSi_{A_{ex}}O_{(A_{ex}+D)}(OH)_{(2A_{ex}-2D+4)} + (2A_{ex} + 2D - 5)H_2O + 2HCl \quad (5)$$

where D is the hydration state of the assumed Na–Al–Si complex.

The Na–Al–Si solutes on the right-hand sides of Eqs. (4) and (5) are most likely a mixture of various polymerized species of unknown stoichiometry, but in each case the bulk solute is assumed to be electrically neutral. Unit Na/Al ratio and essentially Cl-free composition of the Na–Al–Si solutes are also assumed, consistent with the composition of the melt phase (Table 2), which should be a crude guide to subsolidus fluid composition.

The hypothesis that polymerized species are responsible for the reciprocal enhancement of Al and Si solubility is consistent with expected behavior of high P–T fluids (Manning, 2004). For example, the slight modification of solvent properties produced by dilute solution of Al would, by itself, have negligible effect on SiO_2 solubility in H_2O–NaCl fluids. Low pH would have no effect on quartz solubility at elevated P and T (Anderson and Burnham, 1967), so the reciprocal enhancement of SiO_2 solubility must result almost entirely from formation of aluminosilicate complexes, as envisioned by Anderson and Burnham (1983). Na-aluminosilicate polymerization is also consistent with the observation that NaCl enhances the solubility of corundum. In the corundum-saturated, SiO_2-free system at low-P metamorphic conditions and low salinity, the dominant Na–Al species is $NaAlO(OH)_2$ (Anderson and Burnham, 1967) or $NaAl(OH)_4$ (Walther, 2001).

The bulk composition of Na–Al–Si species is only approximately constrained by the present results. The Si/Al ratio (A_{ex}) of the species in Eqs. (4) and (5) varies with X_{NaCl} and with SiO_2 activity. Values of A_{ex} (Table 3) suggest that, collectively, the solutes have a bulk composition near albite stoichiometry in concentrated NaCl solutions at SiO_2 saturation. The hydration state of the solutes is probably dependent upon H_2O activity, so that the parameters B, C and D are indeterminate in this analysis. Burnham and Davis (1974) suggested that the monohydrate, $NaAlSi_3O_8 \cdot H_2O$, is a major mixing component of melts in the system $NaAlSi_3O_8$–H_2O at high P and T, and this hydration state could conceivably apply to concentrated aluminosilicate solutions at conditions approaching the critical curve in the binary system. The quartz- and corundum-saturated Si/Al ratio of ~1 in initially pure H_2O could correspond to a monovalent aluminosilicate complex suggested by Salvi et al. (1998) on the basis of Raman spectroscopy of pH-neutral solutions of boehmite with aqueous silica at 300 °C. It is quite possible that the inferred complexes at high P and T are also charged. From these considerations it is clear that the solubility behavior is a complex function of NaCl, H_2O, and SiO_2 activities, even if the polymeric species are indeed neutral and have unit Na/Al, as assumed. Variable dissociation of polymers would further increase the complexity.

4.5. Al_2O_3 mobility in high-grade metamorphism of peraluminous rocks

Our proposal of Na-aluminosilicate polymerization supports the suggestion of Anderson and Burnham (1983) that solute complexes having nearly feldspar bulk stoichiometry could be important in mobilization of alumina in the crust. These authors, after a comprehensive review of corundum, quartz and alkali feldspar solubility measurements at high pressures and temperatures, qualified their earlier (Anderson and Burnham, 1967) emphasis on the pH control of Al_2O_3 mobility and concluded that Na–Al–Si complexing can also be an important control in rock–fluid systems. Fig. 5 illustrates that Al solubility is at a maximum in the quaternary system Al_2O_3–SiO_2–H_2O–NaCl at X_{NaCl}~0.08–0.10 and quartz (or albite+melt) saturation, which corresponds to conditions expected to be quite common in high-grade metamorphism of peraluminous rocks, such as pelites. Metapelites typically contain quartz and aluminum silicate at high grades, which requires dissolved SiO_2 and Al_2O_3 in a model coexisting pore fluid to lie along the saturation envelope (Fig. 5). In addition, the salinity at the maximum (22–26 wt.% NaCl) is moderate, and has been reported from fluid-inclusions associated with aluminosilicate–quartz segregations (e.g. McLelland et al., 2002). Thus, saline fluids coexisting with aluminum silicates under deep-seated metamorphic conditions will contain significant dissolved Al_2O_3.

Natural examples of aluminum silicate precipitation are commonly explained by invoking an externally derived source of acidity to elevate Al solubility in the fluid phase; however, our results suggest that a different model should also be evaluated in such cases. Consider the example of McLelland et al. (2002) from the northern Adirondack Highlands, New York, U.S.A., where sillimanite–quartz veins occur in peraluminous rocks (mainly metapelites). McLelland et al. (2002) attributed inferred high Al solubility to influx of acidic magmatic fluids, based on models in which low pH produces elevated concentrations of Al^{3+}, $Al(OH)^{2+}$, and/or $Al(OH)_2^+$ (Vernon, 1979; Nabelek, 1997). Oxygen isotope data suggest that some fluids may have originated as near-surface solutions. Thus, the model of McLelland et al. (2002) requires at least two fluids to explain the geochemical data. However, fluid-inclusion data in the same study indicate the presence of highly saline fluids of up to 25 wt.% NaCl equivalent. The results of the present study therefore suggest an alternative model, in which high Al_2O_3 solubility (and low pH) is generated by saline solutions, and the mechanism of Al dissolution (and acidity) is complexing with Na and Si rather than the production of charged Al and Al hydroxide species in the presence of HCl. Such solutions could have originated by reactive flow of externally derived fluids from various sources; that is, they need not have been derived from magmas.

Acknowledgements

The manuscript was substantially improved by the insightful critiques of an anonymous reviewer, Alistair Hack, as well as Alan Thompson, who provided much useful discussion on mobility and speciation of Al_2O_3 in aqueous fluids, and acquainted the authors with numerous papers on the subject. Angelo Antignano, Carrie Menold, Peter Tropper and Jorge Vazquez all assisted with the SEM work. This research was funded by NSF grants EAR-0337170 and 0711521.

References

Ague, J.J., 1994. Mass-transfer during Barrovian metamorphism of pelites, south-central Connecticut. I: evidence for changes in composition and volume. American Journal of Science 294, 989–1057.

Anderson, G.M., Burnham, C.W., 1967. Reaction of quartz and corundum with aqueous chloride and hydroxide solutions at high temperatures and pressures. American Journal of Science 265, 12–27.

Anderson, G.M., Burnham, C.W., 1983. Feldspar solubility and the transport of aluminum under metamorphic conditions. American Journal of Science 283-A, 283–297.

Aranovich, L.Y., Newton, R.C., 1996. H_2O activity in H_2O–NaCl and H_2O–CO_2 solutions at high pressures and temperatures measured by the brucite–periclase equilibrium. Contributions to Mineralogy and Petrology 125, 200–212.

Bethke, C.M., 1996. Geochemical Reaction Modeling: Concepts and Applications. New York, Oxford. (397 pp.).

Bohlen, S.R., Montana, A., Kerrick, D.M., 1991. Precise determination of the equilibria kyanite = sillimanite and kyanite = andalusite and a revised triple point for Al_2SiO_5 polymorphs. American Mineralogist 76, 677–684.

Burnham, C.W., Davis, N.F., 1974. The role of H_2O in silicate melts: II. Thermodynamic and phase relations in the system $NaAlSi_3O_8$–H_2O to 10 kilobars, 700° to 1100 °C. American Journal of Science 274, 902–940.

Carmichael, D.M., 1969. On the mechanism of prograde metamorphic reactions in quartz-bearing pelitic rocks. Contributions to Mineralogy and Petrology 20, 244–267.

Cesare, B., 1994. Synmetamorphic veining: origin of andalusite-bearing veins in the Vedrette di Ries contact aureole, eastern Alps, Italy. Journal of Metamorphic Geology 12, 643–653.

Delany, J.M., Lundeen, S.R., 1989. The LLNL thermochemical database. Lawrence Livermore National Laboratory Report UCRL-21658.

Foster, C.T., 1977. Mass transfer in sillimanite-bearing pelitic schists near Rangeley, Maine. American Mineralogist 62, 727–746.

Fisher, D.M., Brantley, S.L., 1992. Models of quartz overgrowth and vein formation — deformation and episodic fluid-flow in an ancient subduction zone. Journal of Geophysical Research 97, 20043–20061.

Hansen, E.C., Janardhan, A.S., Newton, R.C., Prame, W.K.B.N., Ravindra Kumar, G.R., 1987. Arrested charnockite formation in southern India and Sri Lanka. Contributions to Mineralogy and Petrology 96, 225–244.

Harlov, D.E., Newton, R.C., 1993. Reversal of the metastable kyanite + corundum + quartz and andalusite + corundum + quartz equilibria and the enthalpy of formation of kyanite and andalusite. American Mineralogist 78, 594–600.

Holland, T.J.B., Powell, R., 1998. An internally consistent thermodynamic data set for phases of petrologic interest. Journal of Metamorphic Geology 16, 309–343.

Kerrick, D.M., 1988. Al_2SiO_5-bearing segregations in the Leopontine Alps, Switzerland: aluminum mobility in metapelites. Geology 16, 636–640.

Kerrick, D.M., 1990. The Al_2SiO_5 polymorphs. Reviews in Mineralogy 22, 1–406.

Manning, C.E., 1994. The solubility of quartz in H_2O in the lower crust and upper mantle. Geochimica et Cosmochimica Acta 58, 4831–4839.

Manning, C.E., 2004. The chemistry of subduction-zone fluids. Earth and Planetary Science Letters 223, 1–16.

Manning, C.E., 2007. Solubility of corundum + kyanite in H_2O at 700 °C, 10 kbar: evidence for Al–Si complexing at high pressure and temperature. Geofluids 7, 258–269.

Markl, G., Bucher, K., 1998. Composition of fluids in the lower crust inferred from metamorphic salt in lower crustal rocks. Nature 391, 781–783.

McLelland, J., Morrison, J., Selleck, B., Cunningham, B., Olson, C., Schmidt, K., 2002. Hydrothermal alteration of late to post-tectonic Lyon Mountain Granite Gneiss, Adirondack Mountains, New York: origin of quartz-sillimanite segregations, quartz-albite lithologies, and associated Kiruna-type low-Ti Fe-oxide deposits. Journal of Petrology 20, 175–190.

Mohr, D.M., Newton, R.C., 1983. Kyanite–staurolite metamorphism in sulfidic schists of the Anakeesta Formation, Great Smoky Mountains, North Carolina. American Journal of Science 283, 97–134.

Nabelek, P.I., 1997. Quartz–sillimanite leucosomes in high-grade schists, Black Hills, South Dakota: a perspective on the mobility of Al in high-grade metamorphic rocks. Geology 25, 995–998.

Newton, R.C., Manning, C.E., 2000. Quartz solubility in H_2O–NaCl and H_2O–CO_2 solutions at deep crust–upper mantle pressures and temperatures: 2–15 kbar and 500–900 °C. Geochimica et Cosmochimica Acta 64, 2993–3005.

Newton, R.C., Manning, C.E., 2002. Solubility of silica in equilibrium with enstatite, forsterite, and H_2O at deep crust/upper mantle pressures and temperatures and an activity-concentration model for polymerization of aqueous silica. Geochimica et Cosmochimica Acta 66, 4165–4176.

Newton, R.C., Manning, C.E., 2003. Activity coefficient and polymerization of silica at 800 °C, 12 kbar, from solubility measurements on SiO_2-buffering mineral assemblages. Contributions to Mineralogy and Petrology 146, 135–143.

Newton, R.C., Manning, C.E., 2006. Solubilities of corundum, wollastonite and quartz in H_2O–NaCl solutions at 800 °C and 10 kbar: interaction of simple minerals with brines at high pressure and temperature. Geochimica et Cosmochimica Acta 70, 5571–5582.

Newton, R.C., Manning, C.E., 2007. Solubility of grossular, $Ca_3Al_2Si_3O_{12}$, in H_2O-NaCl solutions at 800 °C and 10 kbar, and the stability of garnet in the system $CaSiO_3$–Al_2O_3–NaCl–H_2O. Geochimica et Cosmochimica Acta 71, 5191–5202.

Newton, R.C., Aranovich, L.Y., Hansen, E.C., Vandenheuvel, B.A., 1998. Hypersaline brines in Precambrian deep-crustal metamorphism. Precambrian Research 91, 41–63.

Salvi, S., Pokrovski, G.S., Shott, J., 1998. Experimental investigation of aluminum–silica aqueous complexing at 300 °C. Chemical Geology 151, 51–67.

Sepahi, A.A., Whitney, D.L., Baharifar, A.A., 2004. Petrogenesis of andalusite–kyanite–sillimanite veins and host rocks, Sanandaj–Sirjan metamorphic belt, Hamadan, Iran. Journal of Metamorphic Geology 22, 119–134.

Shen, A., Keppler, H., 1997. Direct observation of complete miscibility in the albite–H_2O system. Nature, 385, 710–712.

Tropper, P., Manning, C.E., 2007. The solubility of corundum in H_2O at high pressure and temperature and its implications for Al mobility in the deep crust and upper mantle. Chemical Geology 240, 54–60.

Vernon, R.H., 1979. Formation of late sillimanite by hydrogen metasomatism (base-leaching) in some high-grade gneisses. Lithos 12, 143–152.

Walther, J.V., 2001. Experimental determination and analysis of the solubility of corundum in 0.1 and 0.5 m NaCl solutions between 400 and 600 °C from 0.5 to 2.0 kbar. Geochimica et Cosmochimica Acta 65, 2843–2851.

Whitney, D.L., Dilek, Y., 2000. Andalusite–sillimanite–quartz veins as indicators of low-pressure–high-temperature deformation during late-stage

unroofing of a metamorphic core complex, Turkey. Journal of Metamorphic Geology 18, 59–66.
Widmer, T., Thompson, A.B., 2001. Local origin of high pressure vein material in eclogite facies rocks of the Zermatt–Saas zone, Switzerland. American Journal of Science 301, 627–656.
Zotov, N., Keppler, H., 2000. In-situ Raman spectra of dissolved silica species in aqueous fluids to 900 °C and 14 kbar. American Mineralogist 85, 600–604.
Zotov, N., Keppler, H., 2002. Silica speciation in aqueous fluids at high pressures and high temperatures. Chemical Geology 184, 71–82.